



**HAL**  
open science

## Peculiarities of measuring fluorescence decay times by a streak camera for ps-TALIF experiments in reactive plasmas

Laurent Invernizzi, C.Y. Duluard, Hans Höft, Khaled Hassouni, Guillaume Lombardi, Kristaq Gazeli, Swaminathan Prasanna

### ► To cite this version:

Laurent Invernizzi, C.Y. Duluard, Hans Höft, Khaled Hassouni, Guillaume Lombardi, et al.. Peculiarities of measuring fluorescence decay times by a streak camera for ps-TALIF experiments in reactive plasmas. *Measurement Science and Technology*, 2023, 34 (9), pp.095203. 10.1088/1361-6501/acd8db . hal-03886543v2

**HAL Id: hal-03886543**

**<https://hal.science/hal-03886543v2>**

Submitted on 23 May 2023

**HAL** is a multi-disciplinary open access archive for the deposit and dissemination of scientific research documents, whether they are published or not. The documents may come from teaching and research institutions in France or abroad, or from public or private research centers.

L'archive ouverte pluridisciplinaire **HAL**, est destinée au dépôt et à la diffusion de documents scientifiques de niveau recherche, publiés ou non, émanant des établissements d'enseignement et de recherche français ou étrangers, des laboratoires publics ou privés.



Distributed under a Creative Commons Attribution - NoDerivatives 4.0 International License

# Peculiarities of measuring fluorescence decay times by a streak camera for ps-TALIF experiments in reactive plasmas

Laurent Invernizzi<sup>1</sup>, Corinne Y. Duluard<sup>1</sup>, Hans Höft<sup>2</sup>, Khaled Hassouni<sup>1</sup>, Guillaume Lombardi<sup>1</sup>, Kristaq Gazeli<sup>1</sup>, Swaminathan Prasanna<sup>1</sup>

<sup>1</sup> Laboratoire des Sciences des Procédés et des Matériaux, LSPM, CNRS, Université Sorbonne Paris Nord, UPR 3407, F-93430 Villetaneuse, France

<sup>2</sup> Leibniz Institute for Plasma Science and Technology (INP), Felix-Hausdorff-Str. 2, 17489 Greifswald, Germany

E-mail: kristaq.gazeli@lspm.cnrs.fr

## Abstract

We present a detailed methodology for (i) correctly configuring a streak camera to capture raw picosecond two-photon absorption laser induced fluorescence signals (ps-TALIF) of H-atom in low- and atmospheric-pressure plasmas, and (ii) properly processing the recorded raw experimental data with a dedicated mathematical signal processing method to infer actual ps-TALIF signals of H-atom. The goal is the accurate determination of the decay time of the recorded ps-TALIF signals of H-atom. A ps-laser is used to excite atomic hydrogen produced in both plasmas and the raw fluorescence signals are detected by the streak camera using different time windows/ranges (TR). It is shown that the choice of the TR affects the shapes and the decay times of the recorded raw TALIF signals. This is defined as the instrumental function of the streak camera and has a Gaussian profile as determined by recording the ultrafast laser pulse at different TR. To remove this instrumental distortion and extract the actual shape of the TALIF signals, the captured raw TALIF signals were fitted using the mathematical procedure developed in this study, which involved an exponentially modified Gaussian function. The application of our methodology leads to more reliable measurements of hydrogen atoms decay times after respecting the following acquisition conditions: (i) the TR of the streak camera should be sufficiently large to capture the complete (raw) TALIF signal, and (ii) the time width of the instrumental function of the streak camera should be as small as possible compared to the actual decay time of the fluorescence, while ensuring an optimal signal-to-noise ratio. This work demonstrates the remarkable potential of the combination of ps-TALIF and streak cameras in state-of-the-art optical plasma diagnostics.

Keywords: ps-TALIF, streak camera, instrumental function, collisional plasmas, hydrogen fluorescence decay time

## 1. Introduction

Nanosecond Two-photon Absorption Laser Induced Fluorescence (ns-TALIF) has been widely used for the characterization of various types of plasmas. Numerous studies have shown that this diagnostic can be employed to quantify atomic species in their ground states like H [1–3], O [2–4], and N [5–7]. However, in many practical cases the accurate determination of these densities via ns-TALIF is challenging. This happens in strongly collisional environments (from a few tens of mbar up to atmospheric or even higher pressures), where the fluorescence decay time of probed atoms is mostly on ns or even sub-ns timescales. In these cases, the use of ns-TALIF for reliable atomic density measurements can be a limiting factor as the duration of the laser pulse becomes comparable or higher than the decay time of the fluorescing atom. Thus, an ultrafast laser (e.g., using picosecond (ps) or femtosecond (fs) pulse duration) is a better choice. In fact, ultrafast TALIF avoids the need of sophisticated chemical kinetic models which are often adopted in ns-TALIF post-treatment and can introduce additional inaccuracies to the absolute atomic density measurements [1,8]. Therefore, accurate quenching rates of reactive species can only be directly measured from their fluorescence decay signals when the duration of the laser pulse is much smaller than the TALIF decay time.

In addition, the use of an ultrafast detector whose response time is much smaller than the decay time of the signal is essential to effectively resolve fluorescence signal decays in ns and sub-ns timescales. In this context, the exceptional temporal resolution ( $\Delta t$ ) of streak cameras ( $\Delta t < 1$  ps [9]) is a distinct advantage in comparison to PMTs (photomultiplier tubes;  $\Delta t \sim 1$  ns) or ICCD cameras (intensified charge-coupled device, minimal;  $\Delta t \sim 200$

ps). Jonsson *et al.* employed a streak camera to capture ps-Laser Induced Fluorescence (ps-LIF) signals from laser-excited OH and CO in flames [10]. The use of the streak camera allowed for the measurement of the short decay time of both species down to nanosecond (OH) and few hundreds ps (CO) timescales. Besides, streak cameras have been used as detectors to capture fast (ns) and ultrafast (ps) light events in plasmas. For instance, Höft *et al.* [11] employed a streak camera (0.5 ns time window with  $\Delta t \approx 5$  ps) to capture the temporal dynamics of a sub-ns pulsed spark discharge during the initial stages of its development. They also investigated the axial and radial development of a positive streamer in a dielectric barrier discharge revealing a correlation of the radial expansion with the axial propagation of the streamer [12]. Furthermore, Patel *et al.* studied an atmospheric-pressure ns-pulsed plasma by means of a streak camera using time windows between 5 and 100 ns. In this way, they were able to record the fast propagation of the discharge in the gap between the electrodes and distinguish two phases developed after the initiation of the applied voltage, i.e., a first phase between 0 and 15 ns and a second one between 15 and 100 ns [13].

However, the implementation of a streak camera in advanced optical diagnostics and the proper processing of the recorded signals is not straightforward [14,15]. Particularly, the definition of an optimal time window (hereinafter called “time range”) which is sufficient to acquire the full duration of a luminous event, depends on the characteristic timescale of the signal and the peculiarities of the streak camera. Brockhinke *et al.* applied ps-LIF in an Air/N<sub>2</sub>/H<sub>2</sub> flame and measured with a streak camera fluorescence signals from laser-excited OH and H [15]. To capture the full LIF signals they used two different time windows in the streak camera: 10 ns (OH) and 0.5 ns (H). The consideration of the streak camera as a detector was essential for resolving decay times as low as a few ns for OH and a few tens of ps for H. However, even for the lowest time range values offered by typical streak cameras, the measured raw fluorescence signal may significantly differ from the actual fluorescence signal. Consequently, depending on the type of measurement performed, particular attention should be paid to extracting the actual fluorescence signal by removing the instrumental function of the streak camera (depends on the time range value used in the experiment) by means of dedicated deconvolution techniques. Besides, although streak cameras offer fairly low time-resolution in principle, this key-instrumental parameter for ps-TALIF measurements in collisional plasmas is strongly affected by the values adopted for the slit width of the streak. Actually, the selection of the optimal values of the time range and the slit width for a given TALIF experiment is a tradeoff between minimum TALIF signal distortion and maximum signal-to-noise-ratio. The determination of these optimal values is not straightforward and there is, to our best knowledge, neither clear analysis of the effect of these instrumental parameters on the quality of the measurements, nor clear rational methodology that would enable the determination of these parameters in the literature. In fact, very few studies, exclusively (or essentially) on combustion flames, have used streak cameras in ps-TALIF experiments. Moreover, these studies provided very limited information on the detailed measurement methodology and the peculiarities that enter into play and determine the quality of the measurements when using streak cameras (e.g., reference [15]). Performing such a detailed analysis and setting up a clear rational measurement methodology that guarantees high quality ps-TALIF measurements is the objective of the present work.

More precisely, we employed a ps-laser and streak camera system to determine the fluorescence decay time of laser-excited atomic hydrogen generated in two representative types of low- and high-collisional quenching media, i.e., a low-pressure microwave discharge and an atmospheric-pressure plasma jet, respectively. Application of ps-TALIF for laser-excited H-atom decay time determination is particularly beneficial owing to the short decay times of the fluorescing state in various plasma conditions. Our goals are: (i) to identify the proper time ranges of the streak camera that allow capturing different TALIF signals in each plasma, (ii) to determine and remove the effect of the corresponding instrumental function of the streak on the TALIF signal properties, and (iii) to demonstrate that a streak camera can be a suitable detector for ps-TALIF measurements in reactive plasmas. The experimental setup of ps-TALIF, plasma source and streak camera is described in section 2. Section 3 is dedicated to the presentation and discussion of the results obtained on TALIF decay time measurements of laser-excited H-atom in both plasmas. The main conclusions are given in section 4.

## 2. Experimental setup

### 2.1. ps-TALIF and streak camera system

The principle of TALIF is discussed in reference [16]. Therefore, only a concise description is provided here. Briefly, atoms in their ground state are excited following the absorption of two identical UV laser photons. Then, the laser-excited atoms release their energy by isotropically emitting spontaneous photons (fluorescence). TALIF is particularly suited for atomic density measurements in plasmas or flames.

In practice, TALIF measurements of reactive atom densities are calibrated by performing the same measurements in noble gasses (such as krypton and xenon) of a known density. Thus, the fluorescence intensity can be related to the absolute density of the species being probed. In the case of atomic hydrogen, the noble gas

used for calibration is krypton (Kr). The equation relating the absolute density of atomic hydrogen to the TALIF signals of H and Kr atoms is the following [1,2,4–7]:

$$n_H = n_{Kr} \frac{\int_t \int_\lambda S_{FH} \eta_{Kr} T_{Kr} \sigma_{Kr} A_{Kr} \tau_{Kr} E_{Kr}^2 \lambda_{Kr}^2}{\int_t \int_\lambda S_{FKr} \eta_H T_H \sigma_H A_H \tau_H E_H^2 \lambda_H^2} \quad (1)$$

Where  $n_X$  is the density of a species  $X$  ( $X$  here refers to H or Kr),  $\int_t \int_\lambda S_{FX}$  is the temporally and spectrally integrated fluorescence signal of  $X$ ,  $\eta_X$  is the quantum efficiency of the detector at the fluorescence wavelength of  $X$ ,  $T_X$  is the transmission of the optics at the fluorescence wavelength of  $X$ ,  $\sigma_X$  is the two-photon excitation cross section of  $X$ ,  $A_X$  is the Einstein coefficient of the transition from the laser-excited level to a lower state of  $X$ ,  $\tau_X$  is the experimentally-measured fluorescence decay time of the laser-excited state of  $X$ ,  $E_X$  is the laser energy selected for probing  $X$  atom, and  $\lambda_X$  is the laser wavelength chosen to perform TALIF measurements at the center of the absorption line of  $X$ .

In equation (1), the quantities  $\int_t \int_\lambda S_{FX}$  and  $\tau_X$  are experimentally determined from raw TALIF signals recorded by means of an appropriate laser and detector system. The choice of the laser and the detector depends on the plasma condition and is crucial for an accurate quantification of  $\tau_X$  [16]. For instance, to be able to record ultrafast TALIF signals in highly collisional environments (i.e., fluorescence decay times down to the ns or even sub-ns timescales), a good practice is to combine ps-TALIF with a ps detector such as a streak camera [9]. This drastically increases the accuracy of the measurement of  $\tau_X$  that is directly linked to the uncertainty on the measured atomic density. Furthermore, even though a streak camera is a straightforward solution for ultrafast TALIF diagnostics, its use to acquire a ps-TALIF signal requires considering its peculiarity in terms of instrumental function that changes with the targeted time range and entrance slit width.

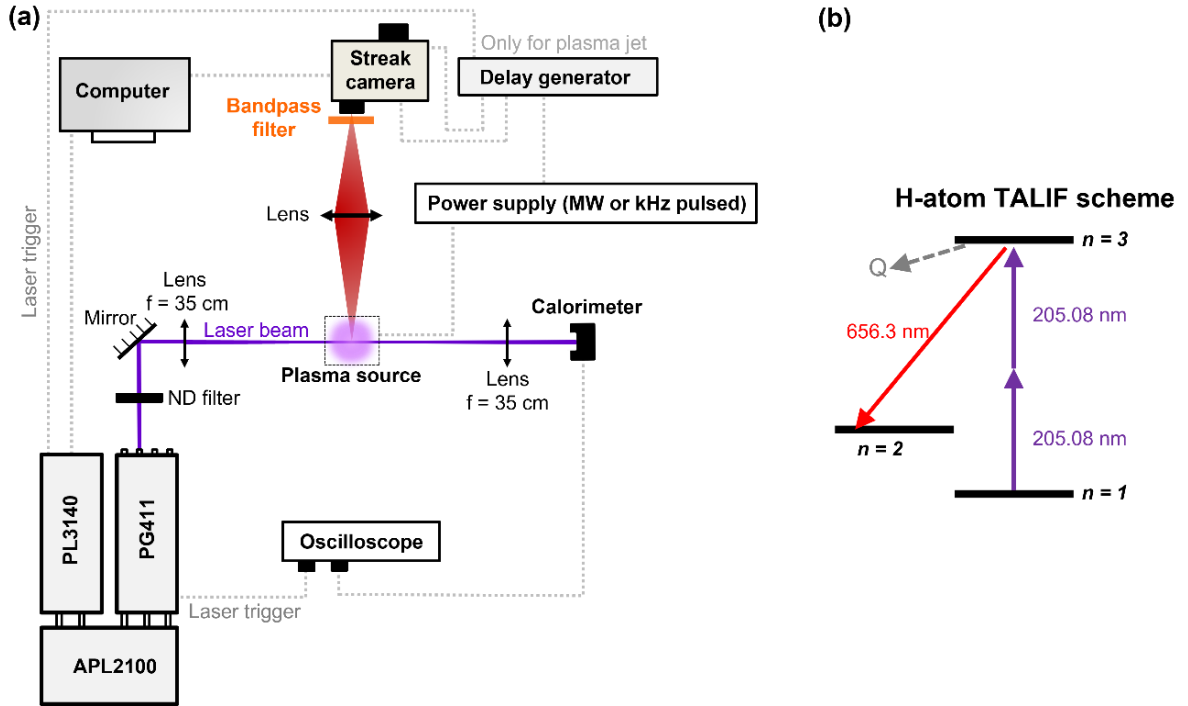


Figure 1: (a) Experimental setup of the ps-TALIF experiments performed in a low-pressure microwave plasma and an atmospheric-pressure plasma jet using a ps laser and a streak camera system. (b) H-atom TALIF scheme comprising two-photon excitation of ground state hydrogen to  $n=3$ , subsequent relaxation to  $n=2$  through fluorescence emission at 656.3 nm (red) and collisional quenching of the laser-excited state (gray).

To perform ps-TALIF measurements in this work, a ps laser from EKSPLA<sup>®</sup> was used. The laser system has been described in detail in [17] and therefore only a brief description is provided here. It is composed of three units: a Nd:YLF pump laser (PL3140), which produces a fundamental output at 1053 nm, a harmonic generator (APL2100) used for fundamental frequency doubling (527 nm) and tripling (351 nm), and a solid state optical parametric generator (PG411) generating ultrafast laser pulses ( $\approx 10$  ps pulse duration; 60  $\mu$ J energy per pulse around 205 nm) in the spectral range 193-2300 nm with a repetition frequency of 5 Hz. The experimental setup is depicted in Figure 1(a) comprising the excitation unit (laser), the detection unit (streak camera; see below),

and two plasma sources used alternatively (here represented as a violet sphere inside a dashed square for simplicity). The excitation and detection scheme is shown in Figure 1(b).

A diaphragm is installed at the output of the PG411 unit of the laser to obtain a circular beam profile. Neutral density filters are placed after the diaphragm to adequately tune the laser energy. In principle, a suitable laser energy ( $E_L$ ) for performing H-atom TALIF should be within a regime where the TALIF signal intensity scales quadratically with  $E_L$  [16,17]. For our laser system, this is the case for  $E_L \leq 14 \mu\text{J}$  per pulse and for  $E_L \leq 57 \mu\text{J}$  per pulse for the low- and the atmospheric-pressure plasma sources, respectively. The  $E_L$  values selected to perform H-atom TALIF experiments are 11 and 38  $\mu\text{J}$  per pulse, respectively. Furthermore, a lens with 35 mm focal length is used to obtain a laser spot with a diameter of 500  $\mu\text{m}$ , which determines the spatial resolution of our TALIF system. After passing through the discharge, the laser beam is collected by another lens with 35 mm focal length and focused on a calorimeter (Coherent J-10MB-LE, 11630V/J) connected to a digital oscilloscope (Lecroy WaveSurfer 10, 1 GHz, 10 GS/s). The fluorescence is collected side-on to the laser's beam direction, avoiding a direct interaction between the laser beam and the detector. The fluorescence is imaged using achromatic lenses with focal lengths of 10 cm (plasma jet) and 20 cm (low-pressure plasma). Finally, a bandpass filter (Semrock FF01-655/15-25) is placed in front of the slit of the detector to remove any stray light coming from the plasma or the surrounding environment.

The detector used is a universal streak camera (HAMAMATSU<sup>®</sup> C10910-05) that can capture light signals down to ps timescales. Among other components, it includes dedicated optics for light focusing on a photocathode where photoelectrons are produced, which are subsequently accelerated, swept, and multiplied by a micro-channel plate (MCP) within the streak tube to finally impact a phosphor screen [9]. There, they are converted back into light that is recorded by means of a readout CMOS camera (ORCA<sup>®</sup>-Flash4.0 V3 C13440-20CU). Streak cameras generally feature distinct time windows for collecting light signals in a specific time range (TR), which is called sweep time, and has values between 100 ps and 1 ms for our streak camera system. The variation of TR is achieved by alternatively using two different sweep units: a "fast" single unit (M10912-01; sweep time: 100 ps to 50 ns; temporal resolution at 100 ps: <1 ps FWHM) or a "slow" single unit (M10913-11; sweep time: 1 ns to 1 ms; temporal resolution at 1 ns: <20 ps FWHM). The time range of the sweep units of the camera is directly connected to the steepness of the voltage ramp applied to the sweep electrodes inside the streak tube to temporally separate the incoming photons. Thus, it is necessary to adapt the time range of the streak camera to the total duration of an incoming light event. The streak camera, the laser, and a pulsed power supply (only used when studying an atmospheric-pressure plasma jet; see below) are synchronized using a 5 Hz TTL signal (internally generated by the laser) and a couple of delay generators (Stanford Research DG645, HAMAMATSU Delay Unit C1097-05). For the fluorescence measurements performed in this study, the entrance slit width of the streak camera has been fixed at 150  $\mu\text{m}$ . The streak camera is operated by a dedicated software installed on a desktop computer. All TALIF signals in this work are recorded using the following parameters: maximum MCP gain=63, number of exposures=20, and CMOS integration time=10 s, resulting in a total acquisition time (TAT) of 200 s for recording one raw TALIF signal. These are the conditions for which the best TALIF signal-to-noise ratios (SNR) were obtained in our experiments. For all the experiments in this work, this ratio was calculated using the formula  $\text{SNR} = (\bar{S} - \bar{B}) / \sigma_{\text{Noise}}$ , where  $\bar{S}$  and  $\bar{B}$  are the spatially averaged TALIF signal and background radiation, respectively, and  $\sigma_{\text{Noise}}$  is the standard deviation of the recorded noise.

## 2.2. Plasma sources under investigation

Our goal is to explore the capacities and peculiarities of using ps-TALIF and, especially, combined with a streak camera in reactive plasma sources which operate in very different pressures. Therefore, two plasma sources are used as testbeds to record ps-TALIF signals by means of a streak camera. First, a microwave plasma reactor, which has been described elsewhere [6], is employed for performing H-atom ps-TALIF measurements at low pressures. It consists of a stainless-steel 6-way cross enclosure with a volume of about 4 L. A microwave plasma is generated in the reactor using a commercial source (Sairem Hi-Wave) detailed in [18]. The microwave power is supplied by a solid-state generator (Sairem GMS 200) through a coaxial cable. The generator delivers a power of 200 W at a frequency varying between 2.4 and 2.5 GHz to obtain the best impedance matching between the source and the discharge. The cavity is pumped by a set of turbo-molecular and rotary pumps (Edwards EXT75DX and Pfeiffer Duo 6M) allowing for the gas pressure to be decreased down to  $10^{-6}$  mbar. The operating gases can be either  $\text{H}_2$  or  $\text{N}_2$ . The pressure in the chamber is measured by a capacitive pressure gauge (Pfeiffer CCR 363) operating in the pressure range  $1.33 \times 10^{-3}$ –13.3 hPa. In this study, pure hydrogen is injected by means of a flow meter (Bronkhorst EL flow) at a constant flow rate of 5 standard cubic centimeters per minute (sccm). Manual control of the primary pump valve allows for the reactor's pressure to be varied from 40 to 200 Pa (typical operating conditions for the Hi-Wave source in this work). Finally, two fused-silica windows are crossed by the laser beam, while a third one (BK7) is located at  $90^\circ$  with respect to the beam. To probe H-atom in this type of plasma, there is no need for synchronization of the laser and streak camera system with the plasma power

supply, i.e., the H-atom density is stationary, since the discharge is driven around 2.45 GHz [6]. The interaction zone between the laser spot and the plasma is located 2 cm below the source.

Besides, an atmospheric-pressure plasma jet is employed for H-atom ps-TALIF measurements under high-pressure conditions. More details on such plasma devices and their applications can be found in reference [19]. The used plasma jet consists of a thin dielectric tube (quartz) wrapped by two ring electrodes, thus forming a dielectric-barrier-discharge configuration. The first ring electrode, which is closer to the tube's outlet, is biased by bipolar square voltage pulses (3.5 kV peak-to-peak) with a repetition frequency of 20 kHz and a duty cycle (i.e., ratio between the pulse width and the period of the voltage) of 50%. The second electrode is directly connected to the power supply's ground potential. The operating gas is helium (99.999% purity) at a flow rate of 1 standard liter per minute (slm) set by means of a mass flow meter (Bronkhorst MV-392-HE). This plasma source does not allow for ignition of plasma in hydrogen. For the helium jet, H-atoms originate in the splitting of water present in the surrounding atmosphere, where the effluent of the jet is interacting with humid air. The plasma source is vertically fixed on an optical table with the helium gas flowing upwards. In this configuration, the laser beam is focused just above the nozzle of the dielectric tube. This allows avoiding reflections from the glass tube that would interfere with the TALIF signal from the plasma. The plasma ignition time ( $t_0$ ) can be set by the trigger of the laser, while the laser pulse starting time is adjustable with respect to  $t_0$  using the abovementioned delay generators. All measurements are performed at the rising edge of the applied voltage pulse where an enhanced production of H-atoms by plasma occurs.

It should be mentioned that using two plasma sources that operate with the same gas at different pressures would be ideal for more direct comparisons. However, this is not feasible because the available plasma sources operate in well-specified voltage, gas, and pressure conditions, as described above. Nevertheless, the choice of the two sources covering two extreme conditions of pressure allows us to demonstrate the challenges with respect to ps-TALIF application.

### **3. Acquisition of ps-TALIF signals using a streak camera and their interpretation method**

In the following subsections, we show how the features of the H-atom TALIF signal (shape, rise time, and decay time) may be affected by the peculiarities of the streak camera with emphasis being put on its time range. It must be noted that a determination of the absolute H-atom densities in both plasmas, their dependence on different plasma conditions as well as the study of their kinetics is out of the scope of the present work.

### 3.1. Instrumental function of the streak camera

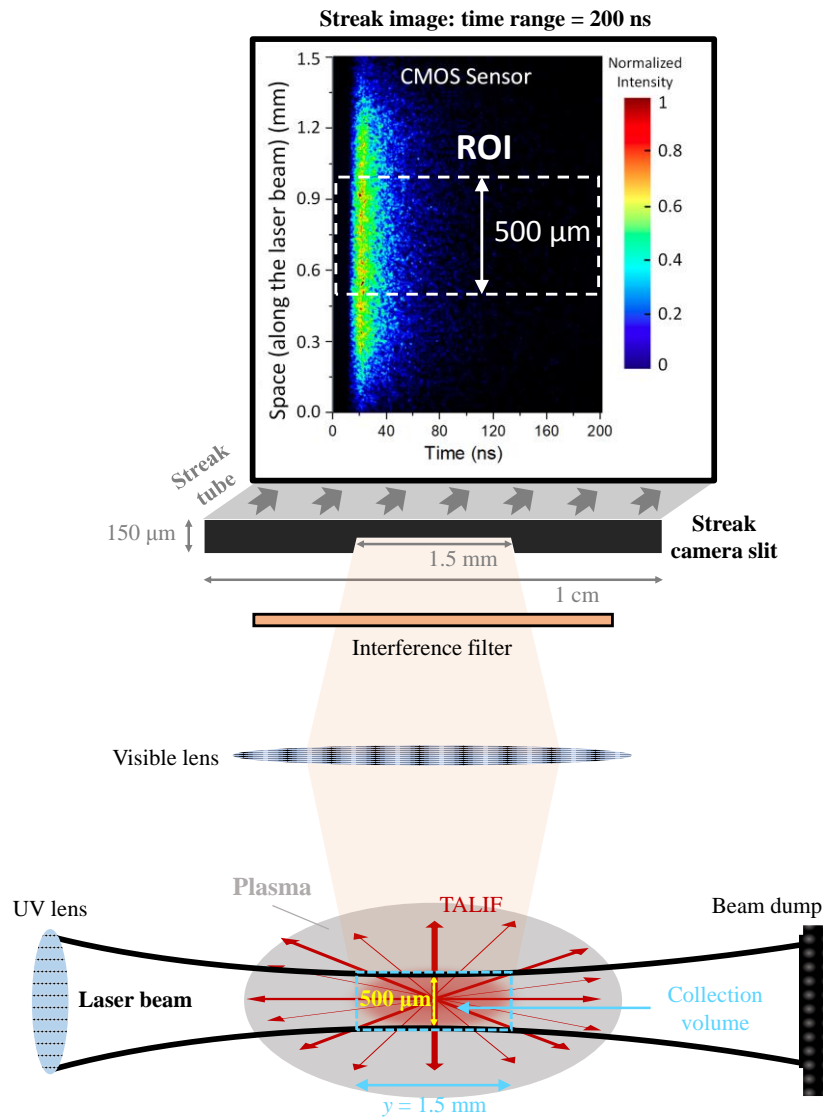


Figure 2: Illustrative scheme of the recording method of H-atom TALIF in a MW low-pressure (200 Pa) plasma with the streak camera. Actually, the raw captured TALIF from the streak camera is a 2D image whose X-axis represents the spatial variation of the signal while the Y-axis represents its temporal variation. An example of a captured streak image is shown on top for TR=200 ns, which is inverted so that the Y-axis of the CMOS sensor (height: 1345 pixels) refers to the spatial variation along the laser beam, and the X-axis (length: 1016 pixels) refers to the time range. For a better comparison, the same region of interest (ROI) is used in the investigation of the two plasma systems. Its size, i.e., 500  $\mu\text{m}$ , is determined by the size of the plasma jet. The recorded TALIF signals are spatially averaged within the dashed white area. The correlation of the time domain of the TALIF signal (ns) with the X-axis of the CMOS sensor is carried out based on the time range set in the camera.

The streak camera employed in this study can capture light events in time ranges varying between 100 ps and 1 ms. This is possible by adapting the sweep time of the fast and slow sweep units. For the experiments presented here, the time range is varied between 200 ps and 500 ns and its effect on the H-atom TALIF signal properties is studied for both plasmas (i.e., TALIF signals are recorded for the same plasma conditions but using different time ranges). A streak image corresponding to the low-pressure plasma is shown in Figure 2 (top). The streak image is a matrix with 1345 horizontal lines and 1016 vertical columns in the CMOS sensor corresponding to the recorded spatial and temporal domains, respectively. Thus, the Y-axis refers to the position on the CMOS sensor, which reflects the physical position of the TALIF measurement. The height of the region of interest (ROI) within the dotted white lines is 500  $\mu\text{m}$ , i.e., equal to the full diameter of the laser spot in the physical discharge space. This ROI was selected to have the same spatial resolution between the two plasma sources considered in this work, as further explained below. Here we must clarify one additional point about the fluorescence collection volume (FCV). As illustrated in Figure 2, to capture the fluorescence signal from the

laser-plasma interaction zone (blue dashed parallelogram), we used an achromatic lens and an interference filter. The focal spot of the lens corresponds to an FCV of  $0.29 \text{ mm}^3$  which has been approximated by assuming a cylindrical laser beam profile with  $1.5 \text{ mm}$  length and  $500 \mu\text{m}$  diameter (i.e., laser beam diameter). This volume is imaged onto the entrance slit of the streak camera as shown in Figure 2. Thus, the full length of the Y-axis of the CMOS sensor in the streak image of Figure 2 represents the full length ( $y=1.5 \text{ mm}$ ) of the FCV in the physical discharge space. For the low-pressure plasma case shown in Figure 2, the total discharge volume is larger than the FCV and, thus, the Y-axis of the CMOS sensor is fully covered by the fluorescence signal. While for the plasma jet, the FCV is about three times lower since the corresponding total plasma volume is much smaller than the low-pressure plasma (the plasma jet has a diameter of about  $500 \mu\text{m}$ ). In this case, the FCV is practically contained in the ROI shown in the streak image of Figure 2. Thus, for a more reliable comparison and to avoid significant spatial averaging in the case of low-pressure plasma, only the fluorescence signals contained in the ROI (about 33% of the area of the entire streak image) were considered. The temporal TALIF signal in this region is spatially averaged over 448 ( $\approx 1345/3$ ) horizontal pixels on the CMOS matrix. Figure 3 shows selected temporal TALIF signals within the ROI of Figure 2. By spatially averaging all the TALIF signals in this region, we calculated weighted averaged TALIF waveforms with corresponding errors, which are appropriately treated to obtain the corresponding fluorescence decay times (see section 3.2).

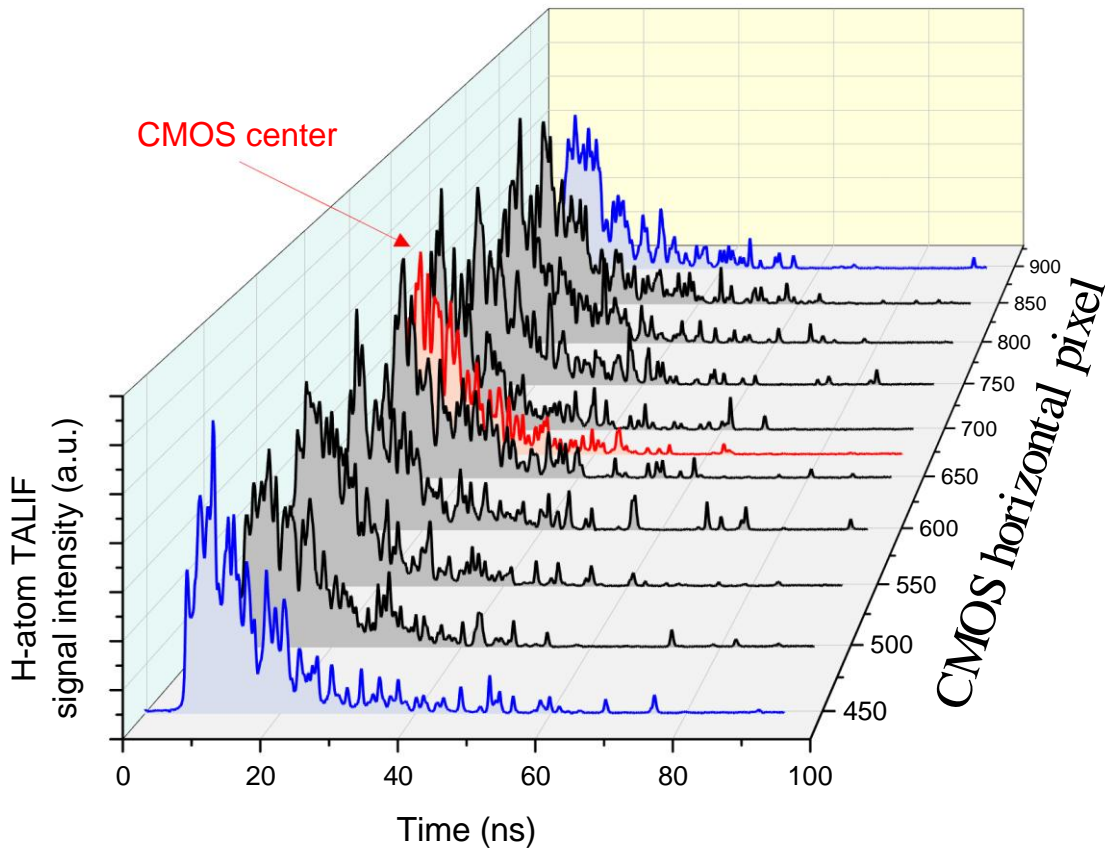


Figure 3: Representative TALIF signals in the ROI denoted with the white dotted lines in the streak image of Figure 2. Each signal refers to a horizontal line (pixel) on the CMOS sensor matrix. These signals are amongst those used ( $\approx 448$  in total) to obtain a spatially averaged TALIF in this ROI (see Figure 4). Blue TALIF signals refer to the edges of the ROI. The red signal is at the central pixel of the ROI and the CMOS sensor.

Figure 4 illustrates spatially averaged TALIF around the center of the CMOS sensor (i.e., region between the dashed lines in Figure 2 containing  $\approx 448$  signals) for different TR for the low-pressure plasma. These results allow for the choice of suitable time ranges that give more reliable raw TALIF signals. This figure reveals that raw TALIF signals can be fully captured by the streak camera only when using  $\text{TR} \geq 100 \text{ ns}$ . Specifically, we can identify two signal regimes which are a fast rising slope followed by a much slower exponential decay. The areas under the full signals are  $(1.28 \pm 0.28) \times 10^9$ ,  $(1.24 \pm 0.30) \times 10^9$  and  $(1.23 \pm 0.39) \times 10^9 \text{ a.u.}$  for  $\text{TR} = 500, 200$  and  $100 \text{ ns}$ , respectively. The small difference between these areas is mainly due to a small decrease of the laser energy during each TAT ( $=200 \text{ s}$ ). In fact, a laser energy fluctuation of 10% over 300 laser pulses (i.e.,  $60 \text{ s} \approx \text{TAT}/3.3$ ) is systematically measured in our experiments.

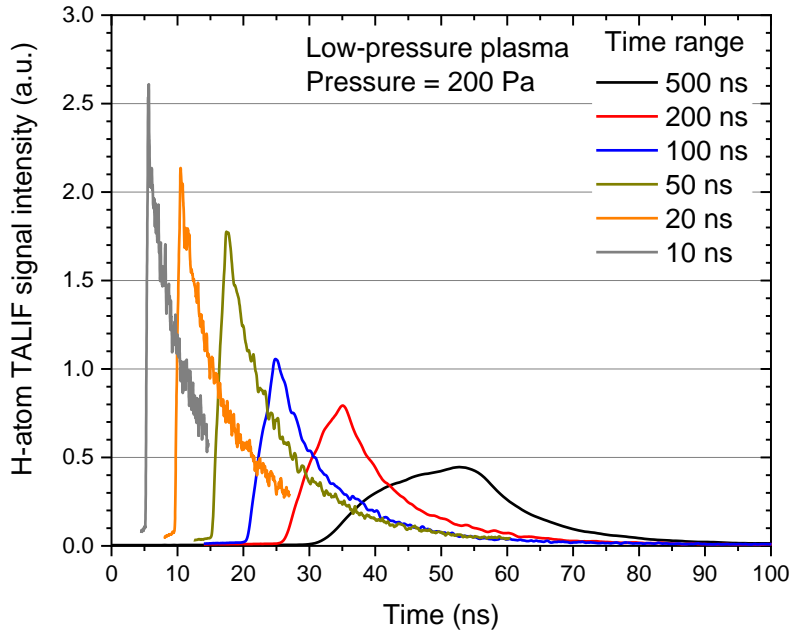


Figure 4: H-atom TALIF profiles obtained from different streak measurements (spatially averaged over the region between the dashed lines, as shown in Figure 2 for different TR. These curves are intentionally shifted in time for a better visualization. These signals are recorded using a slit width of 150  $\mu\text{m}$ .

As can be seen in Figure 4, the overall shape of the TALIF signals significantly changes with increasing TR. As a matter of fact, the rise time of the H-atom TALIF signal in Figure 4 is strongly increased by the variation of the time range of the streak camera. The rise times of the TALIF signal corresponding to each TR are given in Table 1. This distortion is similar to that observed when recording a fast signal with an oscilloscope whose bandwidth is much lower than that of the signal. On the other hand, although the short TR yield better approximations of the rising and early decay phases of the TALIF signal, they do not allow capturing the full fluorescence decay time. One may think that the determination of the actual TALIF signal can be achieved using several smaller TR windows to record the different TALIF portions along the signal's time span and to reconstruct the full signal through a "stitching" process. Unfortunately, this is not feasible due to relatively large fluctuations of the laser energy and the plasma (e.g., emission intensity for the plasma jet) when using multiple small time-ranges instead of a single one. These factors along with the difficulty to identify and set an appropriate starting/ending time for consecutive TR along the TALIF time span, induce undesirable variations on the fluorescence intensity making the "stitching" process impossible. Therefore, proper attention is required towards the significant distortion of the fluorescence signal shape as a function of the TR as seen in Figure 4.

Table 1: Influence of the time range of the streak camera on the rising front duration (expressed in ns and pixels) of the H-atom TALIF. The rise time is measured as the difference between the instants where the TALIF intensity is 10% and 90% of its peak value.

<b>Time range of the streak camera (ns)</b>	<b>500</b>	<b>200</b>	<b>100</b>	<b>50</b>	<b>20</b>	<b>10</b>
<b>H-atom rise time (ns)</b>	14.27	6.60	3.39	1.73	0.81	0.46
<b>H-atom rise time (pixels)</b>	29	36	38	36	38	33

Consequently, a large TR will have poor temporal resolution which will artificially stretch both the rising and the exponential decay phases. However, the rising slope is more affected due to its  $\approx 10$  ps rise time connected to the two-photon excitation as clearly shown in Table 1. Interestingly, no difference is observed when converting the rise time in pixels ( $\approx 35$  px in average). This is due to the constant slit width of 150  $\mu\text{m}$  used for these TR. Therefore, the entrance slit width is also a crucial parameter for setting the temporal resolution of the streak camera. However, for weak fluorescence signals a trade-off between temporal resolution and SNR needs to be considered, since the intensity of the signal is directly proportional to the entrance slit width. In conclusion, there is a significant alteration of the actual fluorescence profile that must be taken into consideration when capturing ps-TALIF signals with a streak camera. The overall effects leading to the distortion of the TALIF signal can be

treated by introducing an instrumental function, similar to the instrumental broadening of an optical spectrometer [20]. The raw TALIF signal collected with the streak camera can be considered as a convolution between its instrumental function and the actual TALIF signal. Since in our case TALIF signal has both ultrafast and fast components for the rising front (few ps) and the decaying part (few ns or hundreds of ps) respectively, the choice of TR as well as the slit width is critical for proper extraction of the actual fluorescence decay times. Therefore, a combination of time range and slit width has to be chosen that allows capturing the full raw TALIF signal with decent SNR.

The instrumental function of the streak camera in our case is experimentally determined using the ultrafast laser pulse as a reference signal. Specifically, we recorded with the streak camera the Gaussian temporal profile of the laser pulse and measured the variation of its FWHM as a function of the time range. For this purpose, the light from the picosecond laser is recorded with the streak camera (only a laser beam reflection is sent into the entrance slit of the streak camera to avoid damage to the camera due to excess light). The jitter of the laser trigger is only a few ps, while that associated with the streak camera and the delay generators used is estimated to be around 25 ps. This prevents in principle the use of the lowest time range provided by the fast sweep unit (i.e., 100 ps) as the laser pulse would easily exit the effective CMOS sensor area. Moreover, a dedicated mathematical process provided in the camera's software allows for a correction of the time-variation of the appearance of the signal in the CMOS sensor due to the jitter [21]. Therefore, the laser pulse temporal profile is recorded using a TR of 200 ps (see Figure 5(a)), and not with a TR of 100 ps. After applying this process, the measured reference laser profile has a FWHM of 9.85 ps obtained by fitting the experimental raw signal with a Gaussian function. This value is in excellent agreement with the laser's manual indicating a pulse duration of about 10 ps at 1053 nm. To investigate the effect of the time range of the streak camera on the measured FWHM of the laser pulse, the laser pulse is recorded using different TR between 200 ps and 500 ns. As mentioned before, besides the TR, the slit width of the streak camera also significantly affects the temporal resolution of the detector. Since the laser pulse is characterized by a large emission intensity (i.e., high SNR), the measurements in Figure 5 are performed with a minimum slit width of 10  $\mu\text{m}$  to achieve the best possible temporal resolution and avoid any additional distortion of the temporal profile of the laser pulse. On the other hand, the choice of a slit width of 150  $\mu\text{m}$  for recording TALIF signals in this work is based on the need of ensuring a good SNR while capturing fluorescence signals in both plasmas.

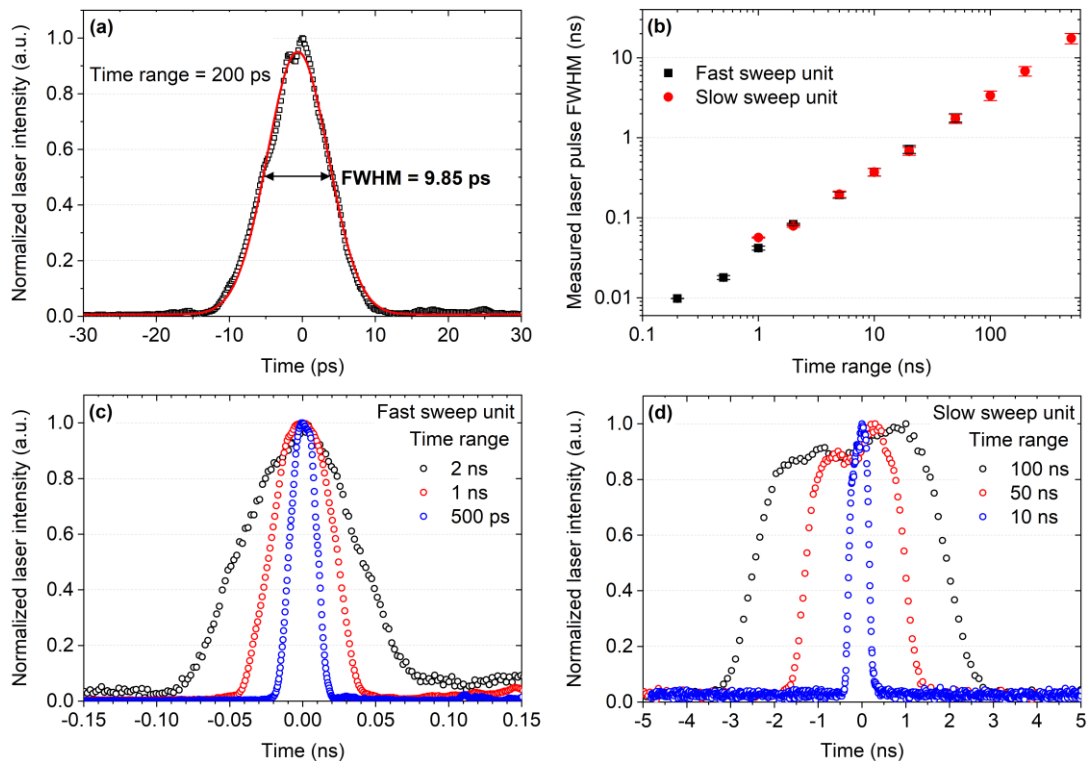


Figure 5: (a) Actual temporal profile of the laser pulse (black squares) recorded by means of the streak camera with the fast sweep unit using a time range of 200 ps and fitted with a Gaussian function (red). (b) Measured FWHM of the laser pulse versus the time range of the streak camera (both the fast and the slow sweep units were used to vary the time range between 200 ps and 500 ns). Representative measured laser pulse profiles referring to TR=0.5, 1, 2 ns (fast sweep unit) and TR=10, 50, 100 ns (slow sweep unit) are illustrated in (c) and (d) respectively. All these measurements were performed with 10  $\mu\text{m}$  slit width of the streak camera.

Figure 5(b) depicts the measured FWHM of the laser pulse as a function of the time range. For  $TR > 0.2$  ns, the corresponding instrumental functions of the streak camera were determined using the ps-laser pulse as a reference signal (Figure 5(a)). More precisely, the recorded broadened temporal laser pulse profile referring to  $TR > 0.2$  ns (Figure 5(c) and Figure 5(d)) can be approximated by a Gaussian function with a corresponding FWHM. Then, this Gaussian profile is taken as the instrumental function of the streak camera at each specific time range. As an example, for  $TR = 10$  and  $100$  ns, the measured temporal profiles of the ps laser by the streak camera, and the corresponding Gaussian fitting functions used to obtain their FWHM are illustrated in Figure 6. Similar fittings on the recorded laser pulses are performed for all  $TR$  studied to obtain their FWHM. These fittings are not shown in Figure 5(c) and Figure 5(d) to make the graph clearer. As depicted in Figure 5 (b), the measured Gaussian FWHM of the laser pulse linearly increases with the increment of the time range. The recorded signal which represents the convolution between the actual laser signal and the instrumental function of the streak camera, is strongly affected by the latter for  $TR$  above  $200$  ps. This means that the actual laser signal can be accurately inferred from the recorded signal only for time ranges below  $200$  ps. The distortion of the temporal profile of the laser pulse with increasing  $TR$  is further clearly illustrated in Figure 5 (c) and Figure 5(d) using representative  $TR$  values ( $0.5 - 100$  ns). To reliably record the full TALIF signals in this work, two different  $TR$  of the slow sweep unit, i.e.,  $100$  and  $10$  ns (Figure 6), were used for each of the two investigated plasmas, i.e., the low- and the atmospheric-pressure plasma, respectively. The corresponding instrumental functions are defined by Gaussian FWHM of  $(0.20 \pm 0.02)$  ns and  $(3.40 \pm 0.45)$  ns, respectively. Our choice of these two  $TR$  values is justified hereafter.

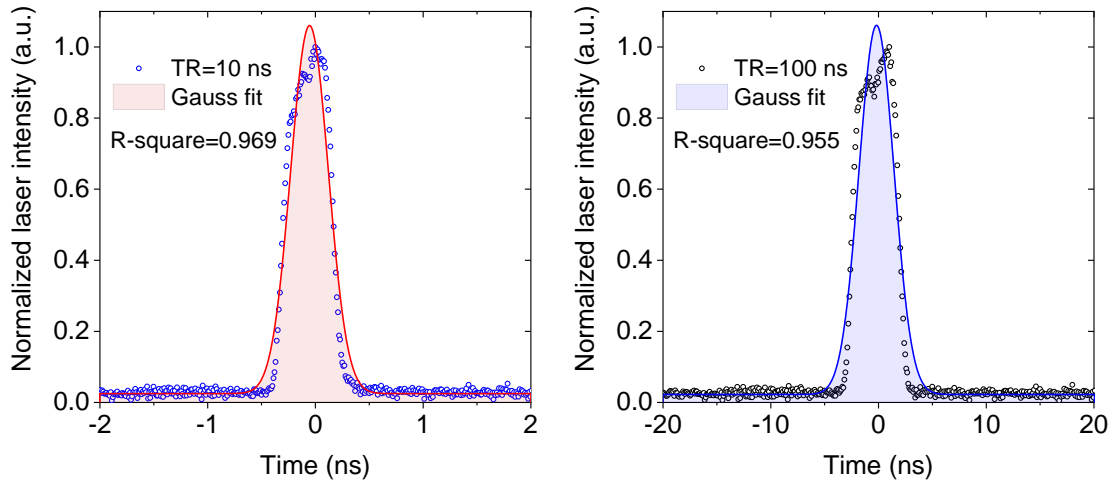


Figure 6: Experimentally measured laser pulse temporal profiles recorded by the streak camera using  $TR = 10$  ns (left; blue circles) and  $TR = 100$  ns (right; black circles). These are fitted with corresponding Gaussian functions (red and blue lines, respectively) to extract their FWHM and obtain the corresponding instrumental functions of the camera.

Furthermore, the effect of the entrance slit width of the streak camera on the temporal resolution of the streak detector is visualized in Figure 7. This figure shows the relation of the slit width and its respective width on the CMOS sensor recorded in the so-called “Focus Mode” of the streak camera (by diffuse-illumination of the slit). In this mode, no sweeping voltage is applied in the streak tube, i.e., the spatial intensity profile on the CMOS sensor is directly connected to the width of the entrance slit. The inset in Figure 7 shows the widths of the profiles (taking the total width of the profile in px, i.e., when the signal is securely above the noise level) as a function of the slit width. Since during the sweep in an actual streak measurement the spatial axis is converted to a time axis, the widths of the intensity profiles on this axis are corresponding to a temporal resolution, i.e., the px value is converted to ns. This was done exemplarily for a  $100$  ns time window shown as the top axis of Figure 7 (since the slit covers only a minor part of the sensor, the axis features a break to show the complete range). In addition, it is clear from the profiles shown in Figure 7 that the intensity is decreasing when reducing the slit width: the selection of a proper slit width is always a trade-off between intensity and temporal resolution.

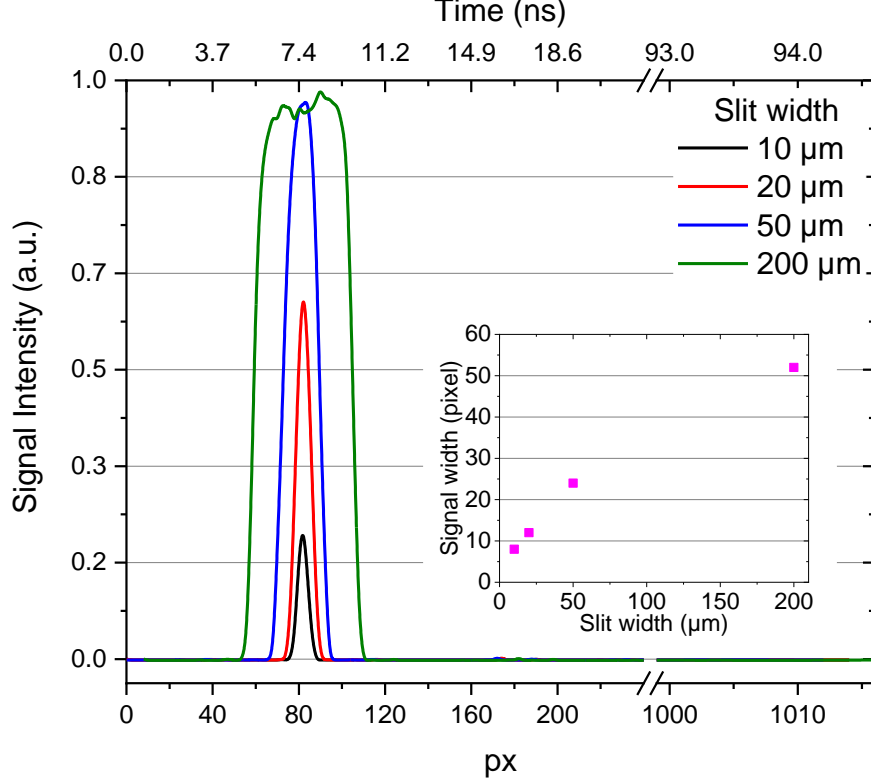


Figure 7: Visualization of the impact of varying entrance slit width on the temporal resolution using the spatial profiles of a diffuse-illuminated slit without the conversion of spatial information to time. This px-to-time conversion was exemplarily performed for a time range of 100 ns. The inset shows the total width of the profile in px, when the signal is securely above the noise level for better comparison.

### 3.2. Interpretation of the fluorescence signals

In section 3.1 we show that the TALIF signal recorded by the streak camera consists of a fast rising slope followed by a much slower exponential decay. More precisely, the TALIF process is characterized by three distinct time regimes:

- (i) a temporal interval before the shooting of the laser pulse represented by the background noise.
- (ii) an ultrafast rising front due to the two-photon excitation process of ground-state atoms covering the laser pulse width (FWHM  $\approx 10$  ps in Figure 5(a)).
- (iii) an exponential decay starting after the previous regime and lasting over a much longer period compared to the laser pulse width.

The intensity of the raw fluorescence signal ( $S_F$ ) entering the streak camera (i.e., falling on the photocathode of the streak camera) can be approximated by a simple analytical function describing the previous three regions [6]. This function, hereinafter referred to as  $S_{FM}$ , consists of the following equations: (2.1) describing the baseline of the TALIF signal (denoted  $A_0$ ; mainly originating from the background noise and lasting up to an instant  $t_0$  where the two-photon absorption takes place; see Figure 8), (2.2) describing a steep rising slope ( $A_1$ ) which corresponds to an ultrafast increase of the TALIF between  $t_0$  and  $t_1$  ( $t_1$  is the instant of the peak intensity of TALIF and  $t_1 - t_0 \approx 10$  ps (laser pulse width, FWHM)), and (2.3) defining an exponential decay from  $t_1$  to the end of the signal, whose time constant is denoted as  $\tau_X$ . These equations are formulated as follows [6]:

$$S_{FM} = \begin{cases} A_0, & t < t_0 & (2.1) \\ A_0 + A_1(t - t_0), & t_0 < t < t_1 & (2.2) \\ A_0 + A_1(t_1 - t_0) \exp\left(-\frac{t - t_1}{\tau_X}\right), & t_1 < t & (2.3) \end{cases}$$

The assumption of a linear steep rising regime is acceptable in the case of ps-TALIF signals owing to the much smaller laser pulse width when compared to the time constant of the exponential decay.

However, due to the limitations of the acquisition system, the signal is modified by the Gaussian profile of the instrumental function of the streak camera as follows:

$$G = \frac{1}{\sigma\sqrt{2\pi}} \exp\left(-\frac{(t-\mu)^2}{2\sigma^2}\right) \quad (3)$$

Where  $\mu$  and  $\sigma$  are the mean and the standard deviation values of the instrumental function, respectively. As a result, the registered final raw TALIF signal with the streak camera is considered as the convolution between the actual TALIF (equations (2.1), (2.2) and (2.3)) and the instrumental function of the detector (equation (3) and Figure 5(b)) i.e.,  $\overline{S}_F = S_{FM} * G$ . Thus, the resulting raw TALIF signal that is recorded by the streak camera becomes:

$$\begin{aligned} \overline{S}_F = A_0 + A_1 & \left\{ \frac{\sigma}{\sqrt{2\pi}} \left( \exp\left(\left(-\frac{(t-t_0-\mu)^2}{2\sigma^2}\right)\right) - \exp\left(-\frac{(t-t_1-\mu)^2}{2\sigma^2}\right) \right) \right. \\ & + \frac{(t-t_0-\mu)}{2} \left( \operatorname{erf}\left(\frac{(\mu+t_1-t)}{\sqrt{2}\sigma}\right) - \operatorname{erf}\left(\frac{(\mu+t_0-t)}{\sqrt{2}\sigma}\right) \right) \\ & \left. + \frac{(t_1-t_0)}{2} \exp\left(\frac{\sigma^2}{2\tau_X^2} - \frac{t-t_1-\mu}{\tau_X}\right) \operatorname{erfc}\left(\frac{t_1-t+\mu+\frac{\sigma^2}{\tau_X}}{\sqrt{2}\sigma}\right) \right\} \quad (4) \end{aligned}$$

In equation (4),  $\operatorname{erf}$  is the error function and  $\operatorname{erfc}$  is the complementary error function. It has to be noted that the convolution between an exponential decay function and a Gaussian profile is nothing but the Exponentially Modified Gaussian (EMG) function. The only difference between equation (4) and the EMG function is the contribution from the linear rise region of the fluorescence. As the TALIF signal rise time is much smaller compared to its decay time, the signal may as well be approximated by a modified exponential decay function. However, for the sake of completeness, we will use equation (4) as the form of the recorded raw TALIF signal with the streak camera. Moreover, the temporal integral of the TALIF signal does not change with the convolution between the normalized instrumental function and the raw TALIF signal. Therefore, the temporal integral of the TALIF signal can be simply expressed as:

$$\int_0^\infty S_{FM}(t) dt = \int_0^\infty \overline{S}_F(t) dt = A_1 \frac{(t_1-t_0)}{2} (2\tau_X + t_1 - t_0) \quad (5)$$

The TALIF signals falling on the central region of the CMOS sensor are used to determine the spatially-averaged temporal profiles (see Figure 2, Figure 3 and Figure 4) and the corresponding standard deviation. Figure 8 shows representative examples of spatially-averaged temporal profiles (black open circles) along with their standard deviations (cyan zones) for the low-pressure microwave plasma (at 40 and 200 Pa) and for the atmospheric-pressure plasma jet. The mean temporal signals are subjected to least-square fitting using equation (4) to obtain the different signal parameters (i.e.,  $A_0$ ,  $A_1$ ,  $\tau_X$ ). The noise of the temporal signal averaged over the spatial dimension of the CMOS sensor, i.e., its standard deviation, has been incorporated into the least square procedure through the instrument weighting of the signal [22]. This allows for an improvement in the confidence of the fit of noisy data. In the fitting procedure, the  $\sigma$  value is assigned to the experimentally determined instrumental function corresponding to the TR. Since the choice of  $\mu$  value of the Gaussian profile does not have a significant impact on the retrieved parameters, as the laser pulse width is much smaller than the TALIF decay time, the  $\mu$  value has been fixed at  $t_0$  coinciding with the beginning of the steep rise front of the TALIF signal. The value of  $\mu$  only induces a time shift on the deconvoluted curve, which does not affect the decay time and the integral under the TALIF signal. Examples of the raw signals  $S_F$  (black circles) and their fitted curves  $\overline{S}_F$  (equation (4); red) are illustrated in Figure 8. Also shown are the constructed actual TALIF signals  $S_{FM}$  (equations (2.1), (2.2) and (2.3); blue) and the Gaussian instrumental functions  $G$  of the streak camera (equation (3); green).

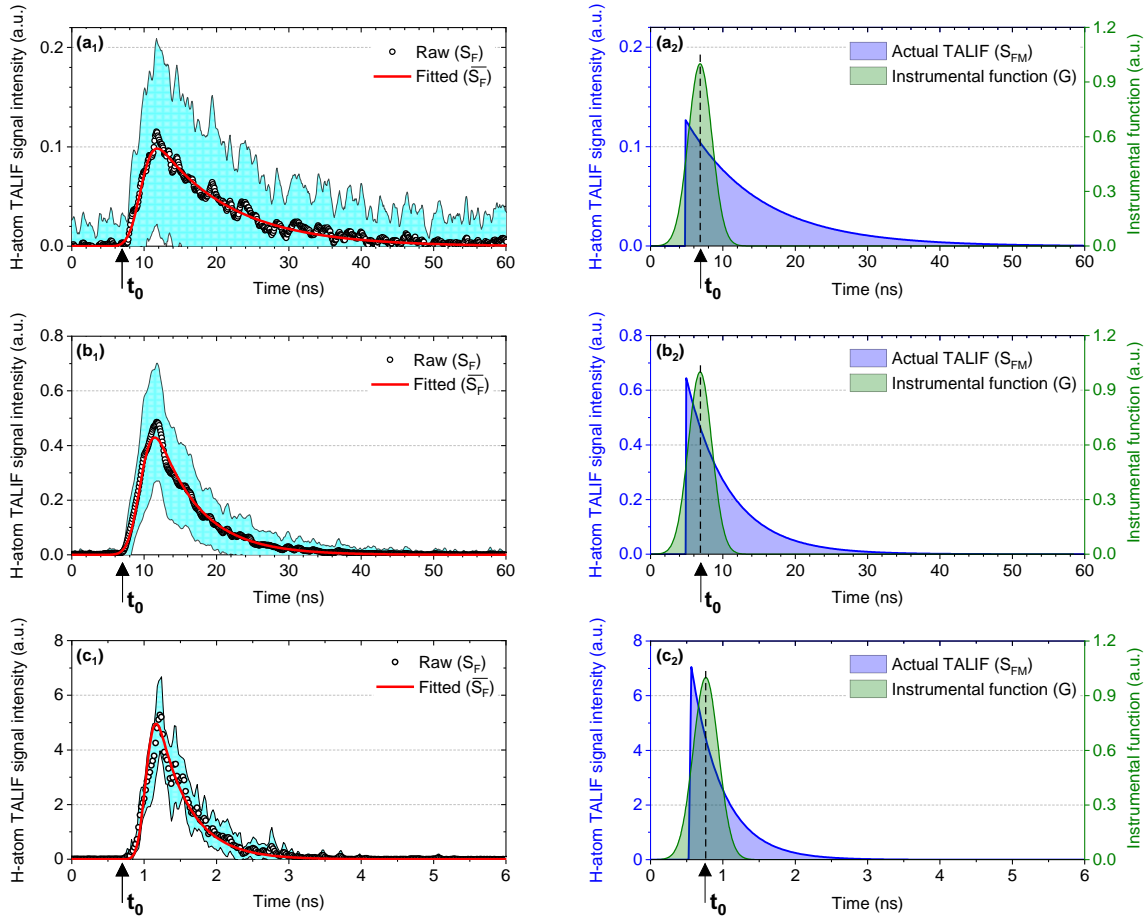


Figure 8: Raw H-atom TALIF signals  $S_F$  (black circles) recorded with the streak camera in the low-pressure microwave plasma at (a<sub>1</sub>) 40 Pa and (b<sub>1</sub>) 200 Pa (TR=100 ns for both), and (c<sub>1</sub>) in the atmospheric-pressure plasma jet (TR=10 ns). These are fitted with theoretical curves  $\overline{S_F}$  (red) based on the procedure developed in this work (equation (4)). As the fitting method considers the weighted error of each point of the raw curve, the corresponding standard deviation is plotted as well (cyan zone). From the features of the theoretical curves, a reconstruction of the actual TALIF signal  $S_{FM}$  (blue) is performed ((a<sub>2</sub>), (b<sub>2</sub>), and (c<sub>2</sub>) respectively). The Gaussian instrumental functions (G) are also shown (green) whose FWHM is 0.20 ns and 3.40 ns for the atmospheric-pressure and the low-pressure plasma respectively.

The ROI designated with the white dotted lines in Figure 2, which is considered to obtain the spatially averaged TALIF signals in Figure 8(a<sub>1</sub>), Figure 8(b<sub>1</sub>) and Figure 8(c<sub>1</sub>), covers 33% of the area of the corresponding streak image and is not defined randomly. Its choice is justified as follows. First, the selected ROI should span around the center of the CMOS sensor, where an optimal performance of the camera is expected. Second, it appears that there is a lower limit on the number of horizontal lines of the CMOS matrix and, thus, the corresponding area of the streak image ( $A_{\min}$ ) that can be utilized to perform the spatial averaging of TALIF. Thus, the selected ROI area cannot be lower than  $A_{\min}$  in order to ensure that the fluorescence decay times obtained from the different fittings are trustful. Figure 9 illustrates the influence on  $\tau_H$  of the ROI area selected to perform TALIF spatial averaging (expressed as % value of the full ROI area in Figure 2). For both plasmas the determined values of  $\tau_H$  seem to reach a saturation threshold for  $A_{\min} \geq 40\%$  ROI. This reveals that the selected area to perform TALIF spatial averaging must cover at least 40% of the ROI area in Figure 2, which allows us to define a confidence zone for the measured  $\tau_H$  values (see Figure 9). Here,  $A_{\min}$  is about 13% ( $\approx 40\% \times 33\%$ ) of the area of the entire streak image and refers to a spatial zone of about 200  $\mu\text{m}$ . These results are obtained using TR=10 ns (plasma jet) and TR=100 ns (low-pressure plasma). However, the present study also focuses on the influence of the time range on  $\tau_H$  (Figure 10), and the TALIF SNR drastically drops at lower TR values. Thus, for all TR considered we used a 2.5 times larger spatial zone referring to the full ROI of Figure 2 and Figure 3. This was done to increase as much as possible the TALIF SNR corresponding to low TR in both plasmas. Finally, by decreasing  $A_{\min}$  below 40% of the selected ROI area we observe a decrease on  $\tau_H$  which is not reasonable due to the large SNR which makes unreliable the fitting of the corresponding TALIF signals. For instance, this decrease is not justified in the case of the low-pressure plasma, which is spatially homogeneous and, thus, we do not expect spatial variations of  $\tau_H$ .

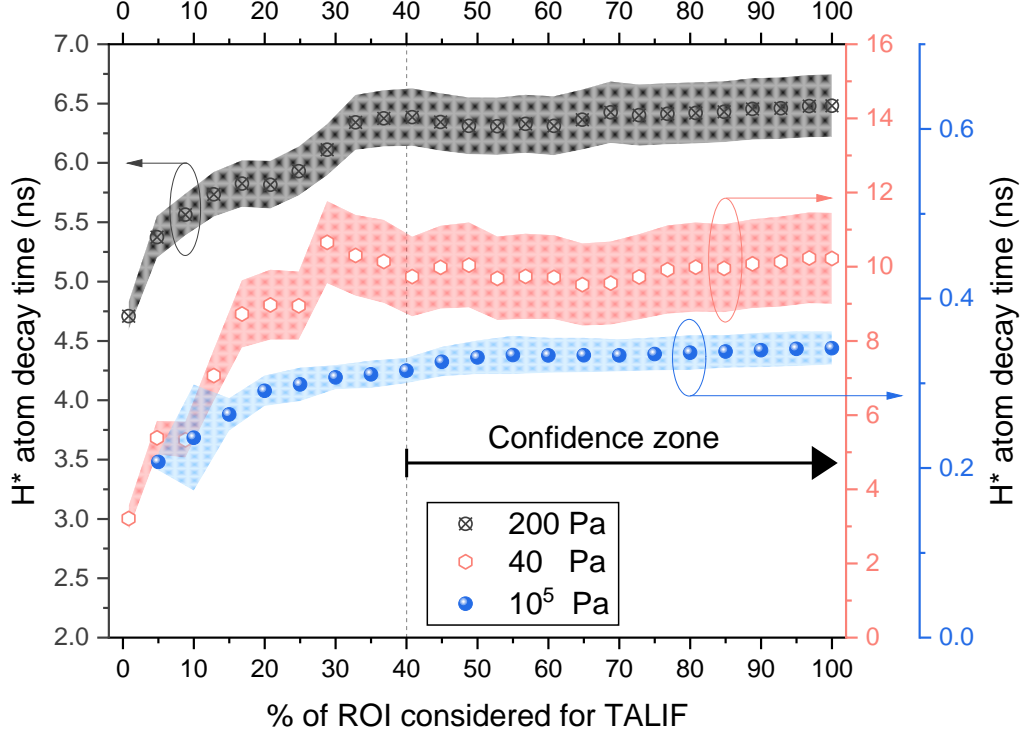


Figure 9: Effect on H\* atom decay time ( $\tau_H$ ) of the area of the ROI selected to perform TALIF spatial averaging. The area chosen is expressed as the % value of the full ROI shown in Figure 2. Both the atmospheric-pressure plasma ( $10^5$  Pa; TR=10 ns; blue) and the low-pressure plasma (200 and 40 Pa shown in black and red, respectively; TR=100 ns) are studied. For both plasmas, the confidence zone for trustful  $\tau_H$  measurement is between 40–50% and 100% of the full ROI area. The standard deviations of the depicted values represent the fitting errors of the weighted TALIF signals obtained from the spatial averaging.

Figure 10 depicts the influence of the time range duration of the streak camera on the measured decay time of the H-atom TALIF signal in the case of a low-pressure plasma at 200 Pa (Figure 10(a)) and an atmospheric-pressure plasma jet (Figure 10(b)). It must be noted that the H-atom decay time here refers to the decay time of the laser-excited state of hydrogen ( $H^*$ ;  $n=3$ ) generated by the absorption of two UV-photons (205.08 nm each). These decay times represent spatially averaged values, which are obtained as follows. First, the weighted averaged TALIF signals (WATS) in each case, i.e., mean waveforms with corresponding standard deviations like shown in Figure 8, are obtained through spatial averaging of all temporal TALIF signals included in the ROI of Figure 2 and Figure 3. The selection of this ROI is explained in Figure 9. Then, these WATS are fitted using equation (4) and the corresponding actual TALIF signals (equations (2.1), (2.2) and (2.3)) are obtained as illustrated in Figure 8(a<sub>2</sub>), Figure 8(b<sub>2</sub>) and Figure 8(c<sub>2</sub>) (blue color). In the latter signals, the decay times of the fluorescence refer to the parameter  $\tau_X$  of equations (2.3) and (4), which is directly obtained from the fitting process along with the corresponding fitting error.

It can be seen in Figure 10(a) (low-pressure plasma) that  $\tau_H$  is significantly rising from 2.2 to 5.7 ns, which corresponds to a TR increase from 10 to 50 ns, respectively. Then,  $\tau_H$  reaches a plateau at about 6.5 ns for TR=100 and 200 ns, while it becomes even larger for TR=500 ns. In Figure 10(b) (atmospheric-pressure plasma jet),  $\tau_H$  oscillates around an average value of about 0.44 ns for TR $\leq$ 20 ns, while it almost doubles at 50 ns and becomes about 2 times larger at 100 ns. These observations clearly demonstrate the effect of the instrumental function of the streak camera as well as the noise on the extraction of H-atoms fluorescence decay times from the raw TALIF signal. For the calculation of the correct decay times from the recorded TALIF signal, its broadening by the instrumental function of the streak camera has to be taken into account. The component of  $\tau_H$  due to the instrumental function decreases when decreasing the TR until it becomes negligible allowing us to reach the true value of the  $\tau_H$  corresponding to the decay of the laser-excited states of H-atom. However, the extraction of  $\tau_H$  is limited by the quality of the signals as well as the ability to capture the full raw signal as seen at low pressures for TR<50 ns. Based on the above description, three regions of  $\tau_H$  variations are identified, as described below.

*Region I:* this region is the most suitable for recording the raw H-atom TALIF in both plasmas in our conditions. It includes moderate TR values indicated by the green hatched zones in Figure 10. In these zones, not only the full raw TALIF signals fit in the CMOS sensor of the streak camera, but also the extraction of the most

reliable approximations of the actual TALIF signals is feasible. This is because the instrumental function of the streak camera is the smallest possible without cutting off any of the signal. However, even within this optimal region the interference with the actual TALIF is still noticeable if one compares the raw and actual TALIF signals in Figure 8. The difference between the shapes of these signals is revealed by applying the mathematical procedure proposed in this study.

*Region II:* lower TR values which are not sufficient for capturing the full TALIF signal (i.e., <100 ns and <10 ns referring to low- and atmospheric-pressure plasmas respectively). The temporal integral cannot be directly determined from the raw signals in these regions. However, it could still be extracted from the fitting of the raw TALIF signal using equation (4). The negative consequence of using the fitting method would be a possible error on H-atom density measurements due to inaccurate extraction of actual TALIF decay times. At low pressures, extraction of  $\tau_H$  is difficult (see, e.g., Figure 10(a)) owing to the higher noise levels (SNR<50). On the other hand, an extraction of more consistent  $\tau_H$  values is possible for the atmospheric-pressure plasma jet (better SNR, due to higher H-atom densities). Consequently, the temporal integrals are much more consistent than in the case of a low-pressure plasma. Nevertheless, one must avoid this region because of the possible uncertainties in the measurement of TALIF decay times and, thus, the atomic densities.

*Region III:* higher TR values (i.e., >200 ns and >20 ns referring to low- and atmospheric-pressure plasmas respectively). Although the full TALIF signal can largely fit in the CMOS sensor or the streak camera, the distortion of the actual TALIF by the instrumental function of the streak camera becomes significant, thus, making the extraction of the actual TALIF decay times through our fitting procedure difficult. Indeed, the actual fluorescence decay time becomes similar to or greater than the FWHM value of the instrumental function of the streak camera. For instance, at TR=500 ns (Figure 10(a)) and TR=100 ns (Figure 10(b)),  $\tau_H/\sigma$  becomes 7.8ns/6.37ns=1.22 and 0.98ns/0.81ns=1.21, respectively. This region should be also avoided for recording the raw TALIF signals.

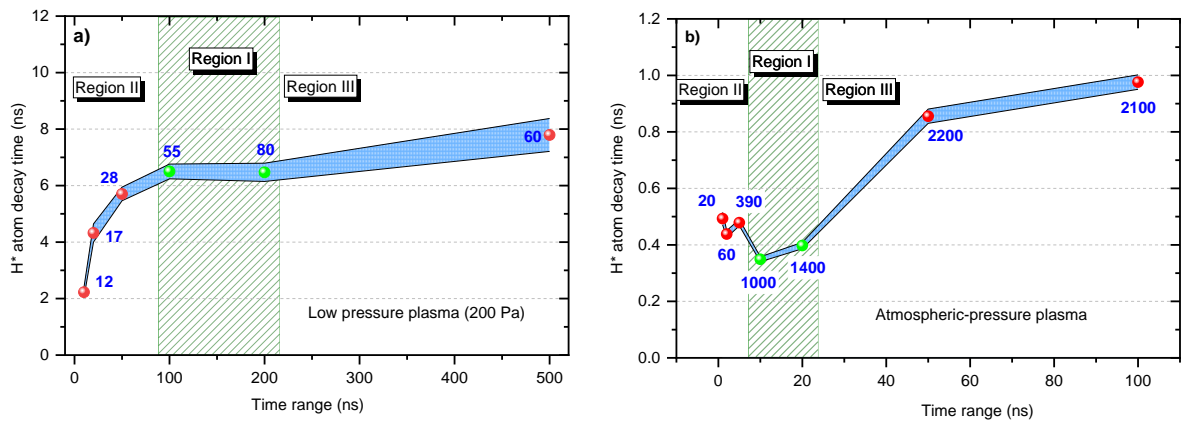


Figure 10: Effect of the time range duration of the streak camera on the measured fluorescence decay time of the laser-excited H-atom ( $H^*$ ) ( $\tau_H$ ) in (a) a low-pressure plasma at 200 Pa and (b) an atmospheric-pressure plasma jet. The values of  $\tau_H$  (red/green spheres) and corresponding standard deviations (blue zone) are obtained through averaging of the TALIF signals over the entire ROI shown in Figure 2, and their subsequent fitting using equation (4). The numbers appearing close to the symbols in both figures refer to the SNR value of each time range.

Based on the above analysis, it can be concluded that for a reliable extraction of fluorescence decay times when performing ps-TALIF experiments combined with a streak camera, one must choose Region I. In conditions where Region I cannot be achieved, Region II could be an alternative compromise provided the raw TALIF signal has a good SNR and a sufficiently long decay. In the present work, the following time ranges from Region I were chosen to measure H-atom decay time: TR=100 ns for the low-pressure plasma and TR=10 ns for the atmospheric-pressure plasma jet. It should be pointed out that  $\tau_H$  does not reach a plateau in Figure 10(b) as it happens in Figure 10(a). The reason we chose Region I in this case as well as for the low-pressure plasma is because it permits us to capture the full duration of the TALIF signal, while at the same time, through our deconvolution method we achieve the highest possible precision on the determination of the TALIF decay and the corresponding integral values (see Figure 11). Furthermore, this is achieved at the lowest possible time range and, thus, lowest distortion by the instrumental function of the streak camera. Choosing Region III instead, although it is feasible in principle because the SNR is high and the TALIF duration largely fits in the TR, the distortion of the TALIF by the instrumental function becomes critical (see Figure 4), making it very complex to extract the actual TALIF with our deconvolution method. Finally, choosing Region II seems to be possible in

some cases where the TALIF signal barely fits in the corresponding TR (e.g., TR=5 ns in Figure 10(b)). In these cases, however, the SNR drastically drops with respect to those obtained in Region I, which makes the application of our deconvolution method less reliable because it is based on the fitting of increasingly noisy signals. Another reason for not choosing Region II is that, for most corresponding TR (e.g., 10 and 1 ns in Figure 10(a) and Figure 10(b), respectively), a portion of the TALIF decay is cut off because it has a larger duration than the TR chosen, as shown in Figure 11(a<sub>1</sub>) and Figure 11(b<sub>1</sub>). This induces undesired errors in the fitting of the TALIF decaying phase. Even if using our deconvolution method to recreate the missing portion of the TALIF signal and “guess” the form of the total actual signal, the calculations of the values of corresponding integrals are questionable when compared to those directly obtained in Region I (Figure 11(a<sub>2</sub>) and Figure 11(b<sub>2</sub>)).

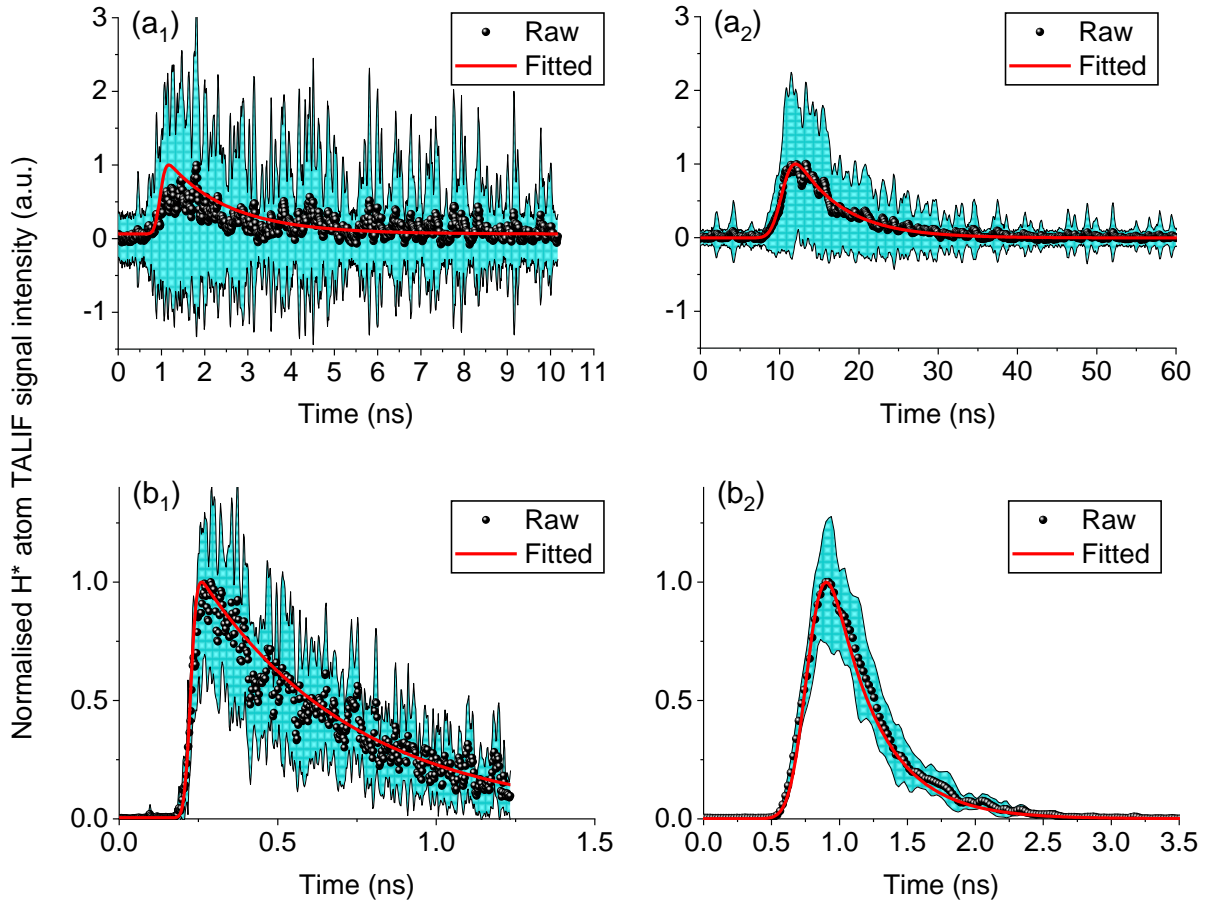


Figure 11: Normalized raw H-atom TALIF signals (black spheres) recorded with the streak camera in the low-pressure microwave plasma at 40 Pa for TR=10 ns (a<sub>1</sub>) and TR=100 ns (a<sub>2</sub>), and in the atmospheric-pressure plasma jet for TR=1 ns (b<sub>1</sub>) and TR=10 ns (b<sub>2</sub>). These are fitted with theoretical curves  $\bar{S}_F$  (red) based on the procedure developed in this work (equation (4)). As the fitting method considers the weighted error of each point of the raw curve, the corresponding standard deviation is plotted as well (cyan). In (a<sub>1</sub>) and (b<sub>1</sub>) a portion of the TALIF decay is cut off because it has a larger duration than those of the TRs chosen, thus making the fitting process more complex.

For investigating the sensitivity of our method, first the pressure in the low-pressure MW-driven discharge was varied between 40 and 200 Pa and the corresponding decay times of the laser-excited state of H-atom (i.e., H\*; n=3) were extracted. This pressure increment already reveals a 1.6-fold decrease in the decay time of hydrogen atoms (i.e., from 10.2 to 6.5 ns according to our measurements) due to a relatively higher collisional frequency at 200 Pa compared to 40 Pa. Second, the method is further considered for TALIF experiments performed in an atmospheric-pressure plasma jet, which represents a reactive medium with a much higher collisional frequency, since its operating pressure is 500 times larger compared to 200 Pa. Thus, a much faster quenching of the laser-excited state is expected in this plasma source. Indeed, our measurements reveal that the corresponding H-atom decay time is drastically decreased to 0.35 ns, i.e., about 19-fold decrease with respect to the value obtained at 200 Pa in the low-pressure plasma, which is in a relatively good agreement with reference [23]. Therefore, our TALIF data treatment method can be applied for extracting laser-excited H-atom decay times in different reactive plasmas operating at least in the range between 40 Pa and atmospheric pressure.

Concerning the different behavior of H\* decay times between Regions I and II in the two plasmas studied, we believe that this is due to the large variations of the corresponding SNR values. Figure 11 illustrates normalized raw H-atom TALIF signals in the low-pressure microwave plasma (40 Pa) (Figure 11(a<sub>1</sub>) and Figure 11(a<sub>2</sub>)), and in the atmospheric-pressure plasma (Figure 11(b<sub>1</sub>) and Figure 11(b<sub>2</sub>)). These signals are shown at the very first TR values in Regions I and II. For the low-pressure plasma, SNR is small and shows similar values in Regions I (Figure 11(a<sub>2</sub>)) and II (Figure 11(a<sub>1</sub>)), thus, the precision of the fitting of the corresponding TALIF signals is rather similar between them. On the contrary, for the atmospheric-pressure plasma, measured SNRs in Region I (Figure 11(b<sub>2</sub>)) are noticeably larger as compared to those of Region II (Figure 11(b<sub>1</sub>)), which makes the fitting of the corresponding TALIF signals easier and more reliable given that the distortion from the instrumental function remains relatively small. Furthermore, the measurement of H-atom densities in both plasmas could be done with the deconvolution method and the good choice of TR, though this is out of the scope of this work. Nevertheless, based on the changes of the  $\tau_H$  revealed in Figure 10, the proper determination of the density of H-atom (inversely proportional to  $\tau_H$  according to equation (1)) strongly depends on the proper selection of the TR, slit width and ROI to determine the actual  $\tau_H$ . For instance, by arbitrary choosing TR=100 ns instead of TR=10 ns (proper value revealed by our analyses) to perform TALIF studies in the case of the atmospheric-pressure plasma jet, the corresponding  $\tau_H$  becomes about 3 times larger and, thus, the H-atom density decreases by a factor of  $\approx 3$ . Therefore, the methodology presented in this work becomes necessary for a proper determination of H-atom densities in plasmas.

Finally, a comparison of our results with similar studies is not straightforward. To the best of our knowledge, there are no published measurements of ps-laser-excited H-atom lifetimes in reactive plasmas using a streak camera. The only known works are references [2,3]. Although they used ps-TALIF as a diagnostic, the fluorescence signals were measured with an ICCD camera. In these works, the reported laser-excited H-atom lifetimes were 0.8 and 1.73 ns, respectively, in atmospheric-pressure plasma jets. The measured lifetimes in our case are much lower (around 0.3 ns for the plasma jet). This is supported by published laser-excited H-atom lifetime measurements in an atmospheric pressure hydrogen-oxygen flame [21] which showcases an advantage of a streak camera against classic ICCD in terms of temporal resolution. However, it is difficult to directly compare the measurements of references [2,3] with ours due to the different conditions of their experiments (reactive medium, laser, camera).

#### 4. Conclusion

This work presents a detailed methodology to infer actual ps-TALIF signals of H-atom in low- and atmospheric-pressure plasmas using a streak camera. Our methodology is based on the combination of advanced ps-TALIF diagnostics with a dedicated mathematical signal processing method. We studied the effect of the time range (TR) of the streak camera on the properties of captured raw TALIF signals (shape, rise time and decay time). The progressive increment of TR led to an increasingly larger distortion of the TALIF envelope. This distortion was due to the contribution of the instrumental function of the streak camera that varies with the value adopted for the time-range. To determine its instrumental function, the streak camera was set to the lowest possible TR (200 ps), and the actual temporal profile of the picosecond laser pulse was measured. This was fitted with a Gaussian function (FWHM $\approx$ 10 ps), which was then used as a reference to determine the distortion on the actual TALIF signal for TR $>$ 200 ps. It was found that to record full raw TALIF signals that better approximate the actual TALIF signals, the smallest possible TR value must be chosen (here, 100 ns and 10 ns for low- and atmospheric-pressure plasmas, respectively). In fact, the choice of a suitable time range depends on the intensity of the signal under investigation, thus, the slit width must be as low as possible to ensure a high temporal resolution while maintaining a decent signal-to-noise-ratio. However, even if using an optimal parameter space to maintain the instrumental function as small as possible, it was still not enough to avoid a distortion on the actual TALIF signal by the instrumental function. It turned out that the application of a dedicated signal post-treatment involving an exponentially modified Gaussian fitting and deconvolution of the acquired signal was mandatory. The implementation of this method led to the extraction of actual TALIF signals and the reliable determination of decay times of H-atoms in both plasmas. An arbitrary selection of the streak camera settings and disregarding the signal post-processing technique proposed in this work can lead to large errors on the H-atom decay time ( $\tau_H$ ) and its absolute density ( $N_H$ ). For instance, choosing TR=100 ns instead of TR=10 ns (proper value revealed by our methodology) to perform ps-TALIF studies in the case of an atmospheric-pressure plasma jet, the corresponding  $\tau_H$  becomes about 3 times larger and, thus,  $N_H$  decreases by a factor of  $\approx 3$ . Therefore, the method presented in this work becomes necessary for a proper determination of ps-TALIF signals in plasmas.

#### Acknowledgments

This work was funded by the ANR ASPEN project (ANR-16-CE30-0004), the ANR ULTRAMAP project (ANR-20-CE51-0020), the DFG project MAID (number 466331904) and the IDF regional project SESAME

DIAGPLAS. The authors would like to acknowledge Dr. D. Stefas and Mr. J. P. Largent for their contribution on the development of a Python code used in the fitting procedure of the raw TALIF signals, Dr. T. Franzl and Dr. I. Grill from HAMAMATSU Photonics Germany, Mr. J. Siue from HAMAMATSU Photonics France for their technical support related to streak cameras, and Dr. C. Anastassiou and Dr. J. Franzke for kindly providing the plasma jet source.

## References

- [1] Mrkvičková M, Ráhel' J, Dvořák P, Trunec D and Morávek T 2016 Fluorescence (TALIF) measurement of atomic hydrogen concentration in a coplanar surface dielectric barrier discharge *Plasma Sources Sci. Technol.* **25** 055015
- [2] Schröter S, Bredin J, Gibson A R, West A, Dedrick J P, Wagenaars E, Niemi K, Gans T and O'Connell D 2020 The formation of atomic oxygen and hydrogen in atmospheric pressure plasmas containing humidity: picosecond two-photon absorption laser induced fluorescence and numerical simulations *Plasma Sources Sci. Technol.* **29** 105001
- [3] Klose S-J, Ellis J, Riedel F, Schröter S, Niemi K, Semenov I L, Weltmann K-D, Gans T, O'Connell D and Helden J H van 2020 The spatial distribution of hydrogen and oxygen atoms in a cold atmospheric pressure plasma jet *Plasma Sources Sci. Technol.* **29** 125018
- [4] Stancu G D 2020 Two-photon absorption laser induced fluorescence: rate and density-matrix regimes for plasma diagnostics *Plasma Sources Sci. Technol.* **29** 054001
- [5] Chng T L, Lepikhin N D, Orel I S, Popov N A and Starikovskaia S M 2020 TALIF measurements of atomic nitrogen in the afterglow of a nanosecond capillary discharge *Plasma Sources Sci. Technol.* **29** 035017
- [6] Bisceglia E, Prasanna S, Gazeli K, Aubert X, Duluard C Y, Lombardi G and Hassouni K 2021 Investigation of N(4S) kinetics during the transients of a strongly emissive pulsed ECR plasma using ns-TALIF *Plasma Sources Sci. Technol.* **30** 095001
- [7] Dumitrache C, Gallant A, Stancu G D and Laux C O 2019 Femtosecond Two-Photon Absorption Laser Induced Fluorescence (fs-TALIF) Imaging of Atomic Nitrogen in Nanosecond Repetitive Discharges *AIAA Scitech 2019 Forum* (San Diego, France: American Institute of Aeronautics and Astronautics)
- [8] Kulatilaka W D, Frank J H and Settersten T B 2009 Interference-free two-photon LIF imaging of atomic hydrogen in flames using picosecond excitation *Proceedings of the Combustion Institute* **32** 955–62
- [9] Hamamatsu Related documents | Streak camera | Hamamatsu Photonics
- [10] Jonsson M, Ehn A, Christensen M, Aldén M and Bood J 2014 Simultaneous one-dimensional fluorescence lifetime measurements of OH and CO in premixed flames *Appl. Phys. B* **115** 35–43
- [11] Höft H, Becker M M, Kolb J F and Huiskamp T 2020 Double-propagation mode in short-gap spark discharges driven by HV pulses with sub-ns rise time *Plasma Sources Sci. Technol.* **29** 085002
- [12] Höft H, Becker M M and Kettlitz M 2018 Correlation of axial and radial breakdown dynamics in dielectric barrier discharges *Plasma Sources Sci. Technol.* **27** 03LT01
- [13] Patel K, Saha A, Zhou T, Meyer T R, Bane S and Satija A 2022 Spectrally filtered ps–ns emission dynamics of atmospheric-pressure nanosecond pulsed plasmas *Appl. Phys. Lett.* **120** 014101
- [14] Rastegari A, Diels J-C, Kamer B, Liu L R, Liu L R, Arissian L and Arissian L 2022 Measurement of delayed fluorescence in  $N_2^+$  with a streak camera *Opt. Express, OE* **30** 31498–508
- [15] Brockhinke A, Bültner A, Rolon J C and Kohse-Höinghaus K 2001 ps-LIF measurements of minor species concentration in a counterflow diffusion flame interacting with a vortex *Appl Phys B* **72** 491–6

- [16] Gazeli K, Lombardi G, Aubert X, Duluard C Y, Prasanna S and Hassouni K 2021 Progresses on the Use of Two-Photon Absorption Laser Induced Fluorescence (TALIF) Diagnostics for Measuring Absolute Atomic Densities in Plasmas and Flames *Plasma* **4** 145–71
- [17] Gazeli K, Aubert X, Prasanna S, Duluard C Y, Lombardi G and Hassouni K 2021 Picosecond two-photon absorption laser-induced fluorescence (ps-TALIF) in krypton: The role of photoionization on the density depletion of the fluorescing state Kr 5p'[3/2]2 *Physics of Plasmas* **28** 043301
- [18] Latrasse L, Radoiu M, Nelis T and Antonin O 2017 Self-matching plasma sources using 2.45 GHz solid-state generators: microwave design and operating performance *Journal of Microwave Power and Electromagnetic Energy* **51** 237–58
- [19] Brandt S, Klute F D, Schütz A and Franzke J 2017 Dielectric barrier discharges applied for soft ionization and their mechanism *Analytica Chimica Acta* **951** 16–31
- [20] Valenti J A, Butler R P and Marcy G W 1995 Determining Spectrometer Instrumental Profiles Using FTS Reference Spectra *Publications of the Astronomical Society of the Pacific* **107** 966–76
- [21] Brandenburg R, Bogaczyk M, Höft H, Nemschokmichal S, Tschiersch R, Kettlitz M, Stollenwerk L, Hoder T, Wild R, Weltmann K-D, Meichsner J and Wagner H-E 2013 Novel insights into the development of barrier discharges by advanced volume and surface diagnostics *J. Phys. D: Appl. Phys.* **46** 464015
- [22] Garrett S J 2015 Chapter 13 - Introductory Numerical Methods *Introduction to Actuarial and Financial Mathematical Methods* ed S J Garrett (San Diego: Academic Press) pp 411–63
- [23] Agrup S, Ossler F and Aldén M 1995 Measurements of collisional quenching of hydrogen atoms in an atmospheric-pressure hydrogen oxygen flame by picosecond laser-induced fluorescence *Appl. Phys. B* **61** 479–87